

LETTER • OPEN ACCESS

Increasing spring dust storms in the future over the Taklimakan Desert, Northwest China: implications from changes in circulation pattern frequency in CMIP6

To cite this article: Rui Mao *et al* 2021 *Environ. Res. Commun.* **3** 111002

View the [article online](#) for updates and enhancements.

You may also like

- [The time interval distribution of sand–dust storms in theory: testing with observational data for Yanchi, China](#)
Guoliang Liu, Lizhen Hao and Feng Zhang
- [Impact of drought on dust storms: case study over Southwest Iran](#)
Mostafa Javadian, Ali Behrangi and Armin Sorooshian
- [Wind-blown dust and its impacts on particulate matter pollution in Northern China: current and future scenarios](#)
Song Liu, Jia Xing, Shovan Kumar Sahu *et al.*

Environmental Research Communications



LETTER

OPEN ACCESS

RECEIVED
5 July 2021REVISED
5 November 2021ACCEPTED FOR PUBLICATION
9 November 2021PUBLISHED
25 November 2021

Original content from this work may be used under the terms of the [Creative Commons Attribution 4.0 licence](#).

Any further distribution of this work must maintain attribution to the author(s) and the title of the work, journal citation and DOI.



Increasing spring dust storms in the future over the Taklimakan Desert, Northwest China: implications from changes in circulation pattern frequency in CMIP6

Rui Mao^{1,2,*} , Dao-Yi Gong^{2,3}, Seong-Joong Kim⁴ , Qi Zong⁵, Xingya Feng³ and Xiao-Xiao Zhang⁶¹ School of National Safety and Emergency Management, Beijing Normal University, Beijing 100875, People's Republic of China² State Key Laboratory of Earth Surface Processes and Resource Ecology, Beijing Normal University, Beijing 100875, People's Republic of China³ Faculty of Geographic Sciences, Beijing Normal University, Beijing 100875, People's Republic of China⁴ Division of Atmospheric Sciences, Korea Polar Research Institute, Incheon 406-130, Republic of Korea⁵ College of Global Change and Earth System Science, Beijing Normal University, Beijing 100875, People's Republic of China⁶ State Key Laboratory of Desert and Oasis Ecology, Xinjiang Institute of Ecology and Geography, Chinese Academy of Sciences, Urumqi, 830011, People's Republic of China

* Author to whom any correspondence should be addressed.

E-mail: Mr@bnu.edu.cn**Keywords:** dust storms, CMIP6, Taklimakan Desert, subtropical westerly jet stream, circulation pattern frequencySupplementary material for this article is available [online](#)

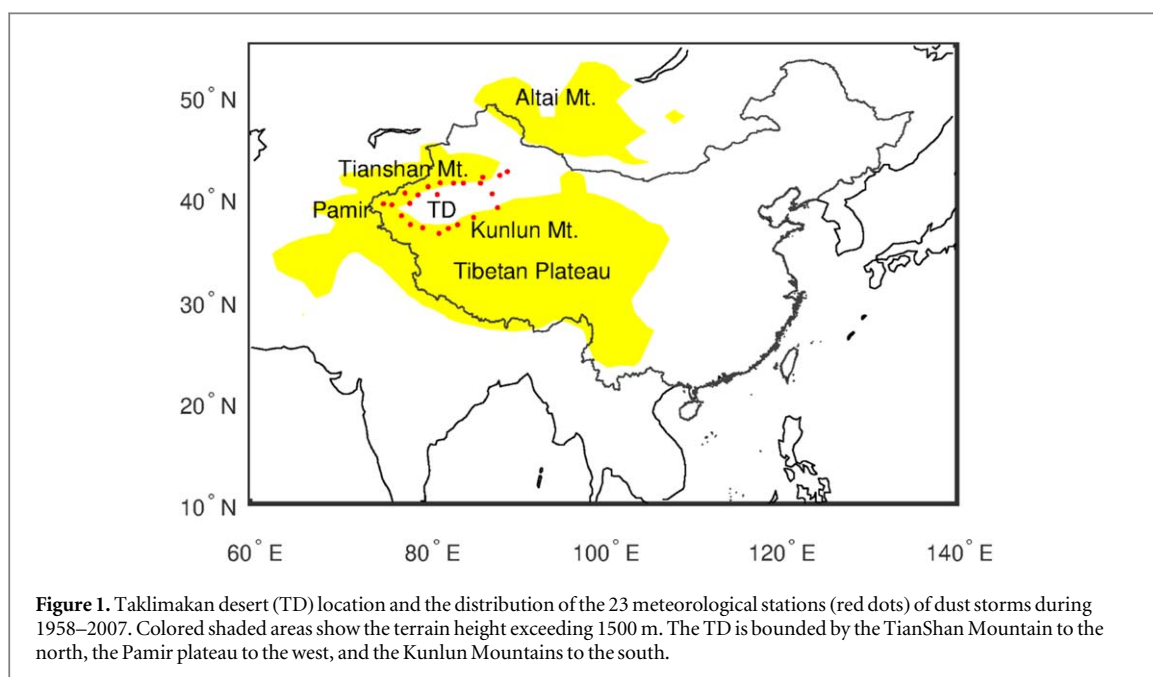
Abstract

Dust storms over the Taklimakan Desert (TD), Northwest China, not only influence human health but also affect regional climate through direct effects of dust aerosols on solar and longwave radiation. The Coupled Model Intercomparisons Project Phase 5 (CMIP5) models project a decrease in dust storms because of a decrease in dust emissions over the TD in the future under warming scenarios. However, inaccurate simulations of dust emissions cause the CMIP5 models to simulate dust storms poorly. Here we analyzed typical circulation patterns that initiate dust storms over the TD and examined changes in the frequency of typical circulation patterns derived from the CMIP6 models in an extreme warming scenario. The results show that there will be an increase in typical circulation pattern frequency in the latter half of the 21st century compared with 1958–2014, implying an increase in dust storms over the TD in the future under the extreme warming scenario. The increase in dust storms over the TD may be related to an increase in synoptic activities in the future from the Middle Asia to the TD, which is caused by a southern movement of subtropical westerly jet stream under the extreme warming scenario.

1. Introduction

The Taklimakan Desert (TD), Northwest China, located in the Tarim Basin, is bounded by the TianShan Mountain to the north, the Pamir plateau to the west, and the Kunlun Mountains to the south (figure 1). The TD is a key source of dust in the atmosphere in the world due to its high elevation and frequent dust storms (Sun *et al* 2001 Zhang *et al* 2003, Huang *et al* 2007, Uno *et al* 2009, Chen *et al* 2013, Zhao *et al* 2013). The dust produced by the TD could influence regional climate by modifying direct effects on solar and longwave radiation and indirect effects on cloud microphysical processes (Han *et al* 2009, Uno *et al* 2009, Chen *et al* 2013).

Dust storms frequently occur in spring over the TD (Zhao *et al* 2013). Synoptic activity in the middle troposphere is a direct factor in initiating dust storms over the TD by providing cold winds into the TD. Aoki *et al* (2005) classified three types of synoptic-scale circulation pattern in the middle troposphere that were linked to dust storms over the TD in spring. These types revealed a trough located to the northeast, to the north, and to the



west of the TianShan Mountains, respectively, resulting in easterly, northerly, and westerly cold winds across the TD and causing dust storms over the TD.

Some works studied changes in dust activities in the future over the TD. Based on the Coupled Model Intercomparisons Project Phase 5 (CMIP5) simulations, a multi-model ensemble mean (MME) of dust emissions and dust optical depth will decrease significantly in the future over the TD in the warming scenarios (Tsunematsu *et al* 2011, Kim *et al* 2014, Pu and Ginoux 2018, Zong *et al* 2021). However, it is inaccurate to derive changes in dust storms from the MME of dust emissions and dust optical depth, since there are large uncertainty in the simulations of dust emissions and dust optical depth over the TD as calculated from the CMIP5 models (Zong *et al* 2021). For example, the HadGEM2-CC and HadGEM2-ES model showed no dust emissions over the TD during 1979–2005, whereas other models showed a large range in dust emissions over the TD. Moreover, the MME of dust simulations presented a lower dust optical depth over the TD than the Gobi Desert, contradicting the observations. In the observations, dust optical depth is higher over the TD than the Gobi Desert (Zong *et al* 2021). Thus, changes in the MME of dust emissions and dust optical depth under the warming scenarios would not accurately present possible variations in dust storms over the TD in the future.

To present the changes in dust storms over the TD in the future, the present study examined the occurrence frequency of typical circulation patterns in the simulations in the future derived from the CMIP6. Since the dominant role of synoptic-scale circulation in initiating dust storms, we hypothesized that changes in the frequency of typical circulation patterns may reveal variations in dust storms over the TD in the future. The rest of this paper is structured as follows. Section 2 described data and cluster method used in this study. The typical circulation patterns in association with dust storms over the TD in spring were reported in section 3. Then changes in the frequency of typical circulation patterns in spring were examined for a historical period and for future periods derived from the CMIP6. In the section 4, causes of the increase in the frequency of typical circulation patterns in the future was discussed. Finally, a conclusion was shown in section 5.

2. Data and method

2.1. Data

In this study, a severe dust storm dataset from China Meteorology Administration was used. This dataset provided dust storm records of stations during 1954 to 2007, including station code, start time, end time, wind speed, and wind direction of dust storm. To describe dust storms over the TD, we selected 23 stations located in the TD or along the fringe of the TD (figure 1). In order to obtain severe dust storm events over the TD, the number of stations with dust storm occurring were counted day by day over the TD. Zhou and Zhang (2003) indicated that a severe dust storm event should include at least three stations that were reported with dust storm occurring in a day. Following the criteria of Zhou and Zhang (2003), a day with three or more stations of dust storm occurring was set as the initial day of a dust storm event; the number of stations in the following days were examined, and a day with less than three stations of dust storm occurring was set as the end of a dust storm event.

Through this process, 143 dust storm events in spring (March to May) were recognized in 1958 to 2007. Moreover, we constructed a time series of the domain-averaged dust storm frequency over the TD, which was used to verify the reliability of typical circulation pattern frequency in reproducing long-term changes in dust storms. During the constructing process, two conditions were set to remove the influence of stations that had minor dust storms. These two conditions were that (1) the selected stations had a climatological dust storm frequency in spring exceeding 1 day during 1958–2007, and (2) the selected stations had fewer than 5 years of no dust storms in spring during 1958–2007 (Mao *et al* 2011b). On the basis of these conditions, the time series of domain-averaged dust storm frequency over the TD was determined by averaging dust storm frequency of the selected stations. Finally, the Japanese 55-year Reanalysis (JRA-55) datasets (Kobayashi *et al* 2015, Harada *et al* 2016) were employed to describe synoptic-scale circulation in association with dust storms. These datasets provide daily wind field and geopotential height at variable levels in the troposphere during 1958 to 2007 and with a spatial resolution of 1.5 degree.

To examine the changes in the frequency of typical circulation patterns under an extreme warming scenario, daily geopotential height at 500 hPa (Z500) of 13 CMIP6 models under a shared socio-economic pathway scenario with emissions high enough to produce a radiative forcing of 8.5 W m^{-2} in 2100 (SSP5–8.5) was analyzed (O'Neill *et al* 2016). A brief introduction of these 13 models were shown in table S1.

2.2. Method

To derive typical circulation patterns in association with dust storms over the TD, a clustering scheme known as self-organizing maps (SOMs) has been used in this study. The clusters derived from SOM method are more distinctive and more robust than the clusters presented by other method, and often outperforms empirical orthogonal function analysis in the extraction of patterns from datasets (Lee and Feldstein 2013, Bao and Wallace 2015). The SOMs have been used quite successfully in studies of synoptic-scale circulation in temperate latitudes (Bao and Wallace 2015) and climate change in arid areas in China (Jiang *et al* 2018, Wang and Yin 2019). Wang and Yin (2019) identified four homogeneous subregions with coherent precipitation regimes over the Tibetan Plateau by using SOMs in 1900–2014. The results of SOMs satisfactorily displayed the impact of geographical features and atmospheric circulation systems.

The SOM method partitions daily data into a specified number of patterns, referred to as SOM patterns, organized on a ($m \times n$) SOM grid. The SOM patterns are determined by minimizing the Euclidean distance between the SOM patterns and the observed fields, yielding patterns that closely resemble the observations. In the SOM analysis, the user specifies the dimensions of the array of clusters in a two dimensional array in advance (Bao and Wallace, 2015). Therefore, a 2×2 array was set in advance in the SOM analysis. Then high-frequency components of Z500 at the start day of dust storm events were collected and were brought into the SOM analysis. By merit of a butterworth filter, the high-frequency components of Z500 was obtained by filtering Z500 on a time scale of 10 days and only components with periods less than 10 days were remained.

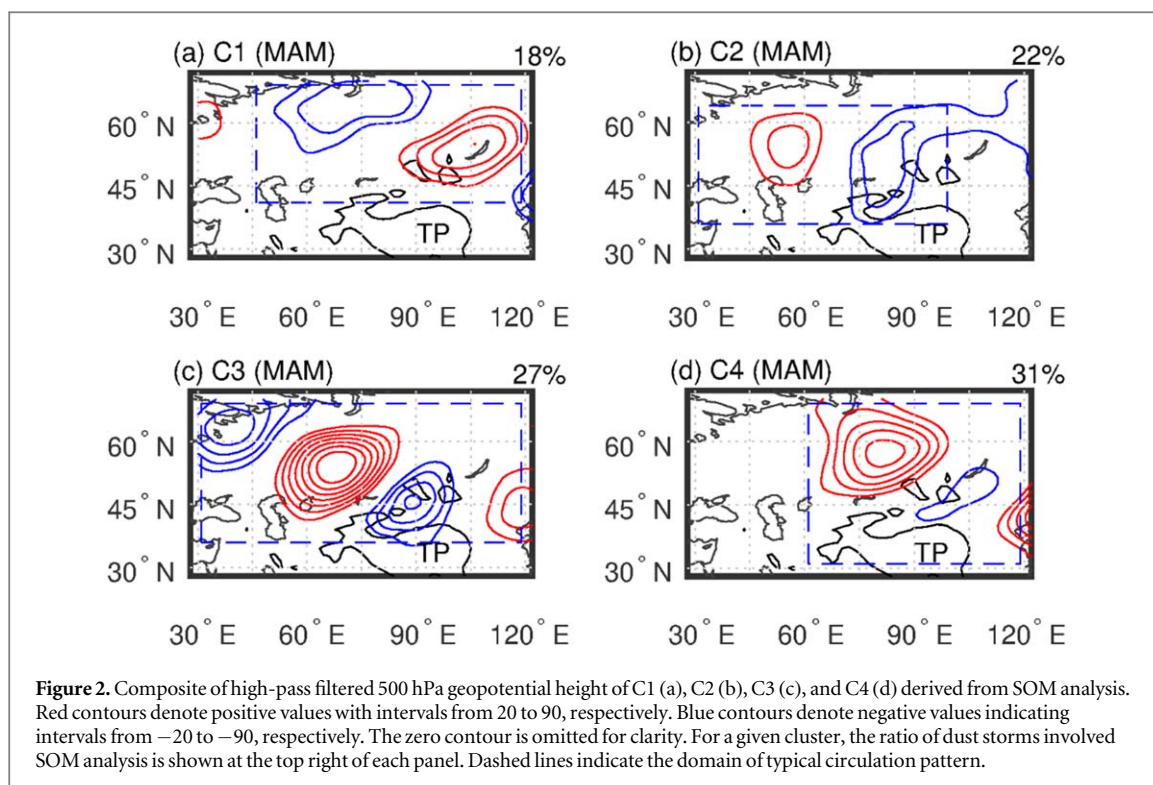
The frequency of typical circulation pattern derived from the SOM analysis was obtained as follows. (1) Daily Euclidean distances between every typical circulation pattern and high-frequency components of Z500 were calculated. Because of different domain of typical circulation patterns, daily Euclidean distance was divided by the number of grid points involved in the domain of every typical circulation pattern. (2) The frequency of every typical circulation pattern was defined as the number of Euclidean distances occurred in the lowest 5% of total daily Euclidean distances, though the threshold of 5% was subjective.

Finally, to explain an increase in dust storms over the TD in the future, we examined synoptic-scale disturbance at 500 hPa level, since synoptic-scale disturbance in the middle troposphere reflects synoptic activity that controls dust storms (Gong *et al* 2006, Mao *et al* 2011a). We used a variance of high-pass filtered Z500 to measure synoptic-scale disturbances.

3. Results

3.1. Typical circulation patterns in spring derived by SOM

Figure 2 shows four clusters in spring derived by SOM using a 2×2 array, which are composite of 18%, 22%, 27%, and 31% of days involved in the SOM analysis, respectively (herein called C1–C4 for simplicity). The clusters are classified into two types: C2, C3, and C4 was featured by a negative Z500 anomaly to the north of the TD and C1 was characterized by a positive Z500 anomaly to the northeast of the Altai Mountains. C1 showed a wave train-like structure from North Europe northeastward across the Ural Mountains to the Baikal Lake southeastward with a negative Z500 anomaly to the east of the Ural Mountains and two positive Z500 anomalies over North Europe and the Baikal Lake. C2 presented a dipole-like structure across the Eurasia with a positive Z500 anomaly to the north of the Caspian Sea and a negative one to the north of the TD. C3 was featured by a northwest-southeast wave-train across the Eurasia, with two positive Z500 anomalies over northern China and



the Middle Asia and two negative ones over North Europe and areas to the north of the TD. C4 resembled the C3. However, the wave-train structure shown in the C3 moved eastward, resulting in positive Z500 anomalies to the north of the Altai Mountains and eastern China and a negative Z500 anomaly to the northeast of the TD. We tested the sensitivity of SOM to the dimensions of the prescribed array of maps using elbow procedures (figure S1 (available online at stacks.iop.org/ERC/3/111002/mmedia)). We compared the sum of square of Euclidean distance among multiple array configurations and found 1×4 and 2×2 are optimal array configurations, because a bend of the elbow occurs at 1×4 and 2×2 array configurations. Therefore, a 2×2 array was confirmed in SOM analysis.

To reveal the cause of dust storms induced by typical circulation patterns, we examined the composite of unfiltered Z500 in the days involved in C1-C4 (figure S2). There was a trough to the northwest of the TD in the C2, to the north of the TD in the C3, and to the northeast of the TD in the C4 in the unfiltered Z500 composites, which were consistent with the negative Z500 anomaly to the north of the TD in the C2-C4 revealed by the SOM. Moreover, we examined the composite of unfiltered 850 hPa wind field (UV850) in the days involved in C2-C4. There were northwesterly winds flowing into the corridor between the Altai Mountains and the Tianshan Mountains and then turning northeastward into the inlet of Tarim Basin because of the blocking effect of the Tibetan Plateau, therefore resulting in dust storms over the TD. Compared to the trough to the northeast of the TD in C4, the trough to the northwest in the C2 and to the north of the TD in the C3 resulted in stronger UV850 crossing the corridor between the Altai Mountains and the Tianshan Mountains, inducing larger UV850 in the TD. The three typical circulation patterns (C2-C4) were reported by Aoki *et al* (2005) as three types of synoptic-scale pattern of dust storm genesis over the TD.

On the contrary to C2-C4, C1 showed a ridge to the northeast of the Altai Mountains and a trough to the far north of the Altai Mountains in the unfiltered Z500 composite. The southwesterly winds associated with the trough turned to be northwesterly winds flowing into the corridor between the Altai Mountain and the Tianshan Mountain due to the blocking effect of the Altai Mountains. Then the northwesterly winds turned northeastward into the inlet of Tarim Basin because of the blocking effect of the Tibetan Plateau. The northwesterly winds in the C1 over the corridor between the Altai Mountains and the Tianshan Mountains were weaker compared to C2 to C4.

3.2. Evaluation of CMIP6 historical simulation of long-term changes in typical circulation patterns

Before we evaluated the performance of the CMIP6 in simulating long-term changes in the frequency of typical circulation patterns, we assessed the reliability of using the frequency of typical circulation patterns to project the long-term changes in dust storms over the TD. The composite of high-pass filtered Z500 of typical circulation patterns from the JRA-55 Reanalysis dataset highly resembled typical circulation patterns derived by SOM

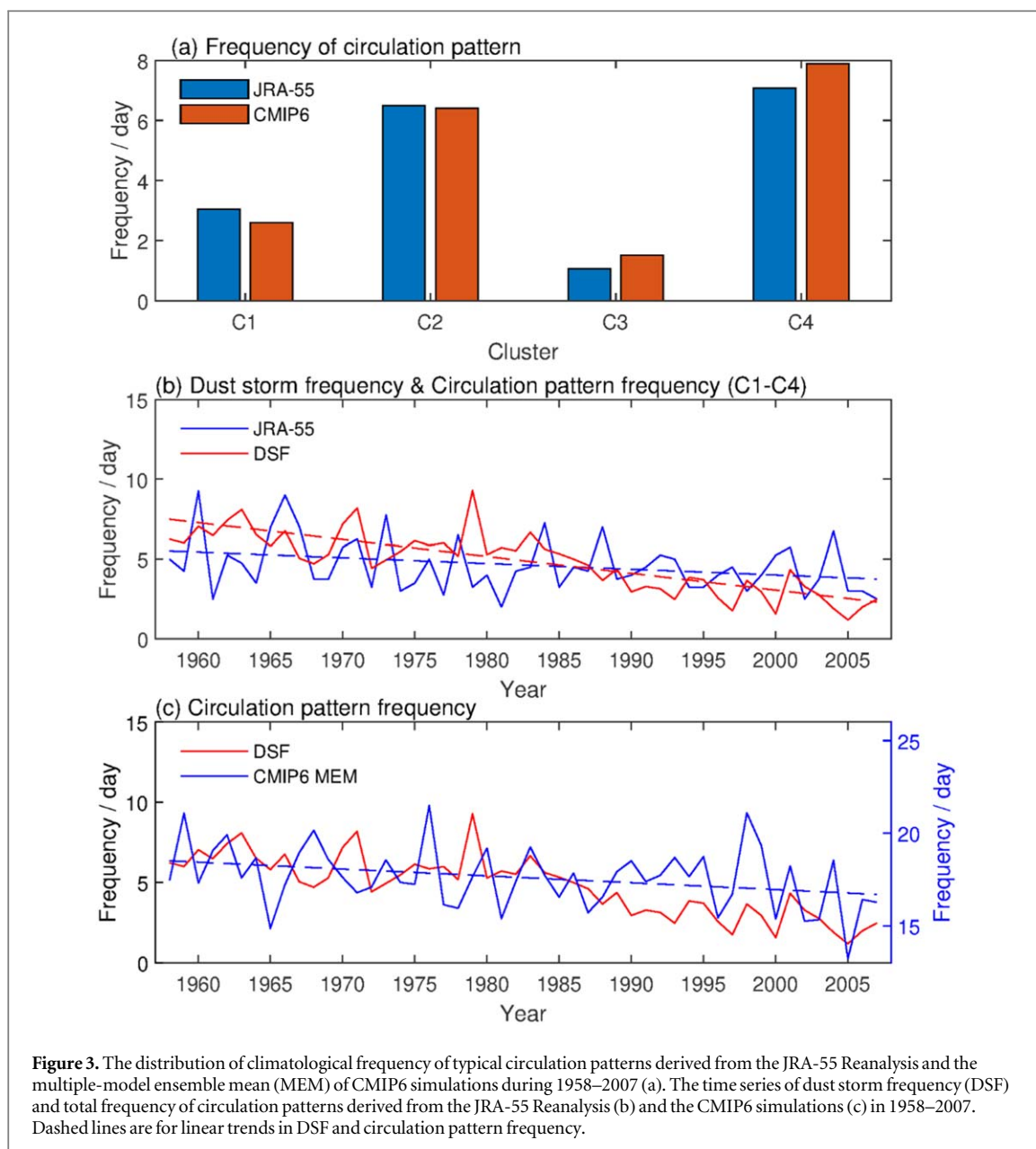
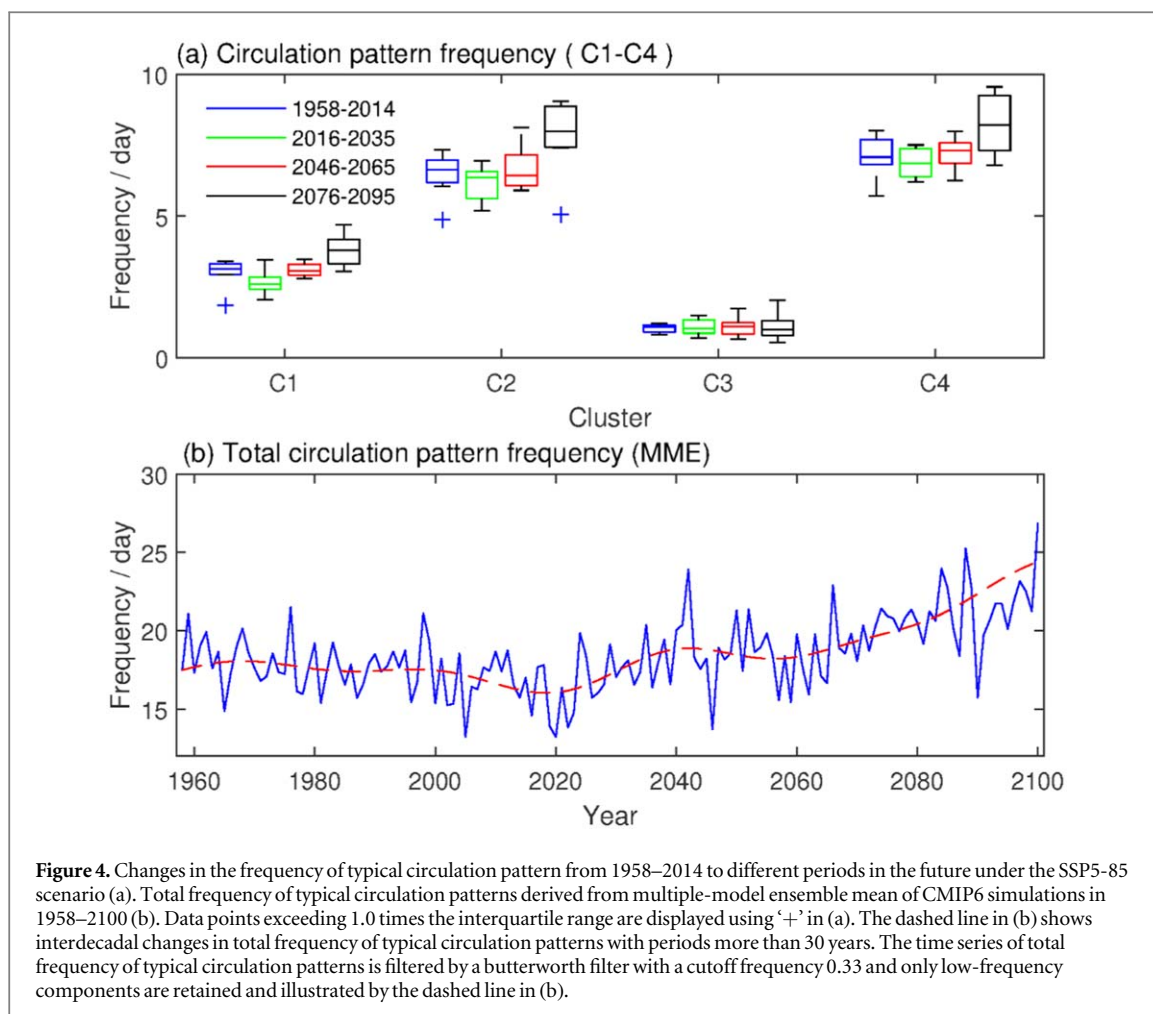


(figure S3). Figure 3(b) shows the time series of observed dust storm frequency (DSF) and typical circulation pattern frequency over the TD derived from the JRA-55 Reanalysis dataset in 1958–2007. Although there were differences in interannual changes between DSF and typical circulation pattern frequency, a decreasing trend in DSF from 1958–2007 was reproduced well by typical circulation pattern frequency. The DSF showed a decreasing trend by -0.1 day per spring during 1958–2007, significant at the 95% confidence level. Compared with the DSF, the total frequency of typical circulation patterns over the TD from the JRA-55 Reanalysis dataset also showed a decreasing trend in 1958–2007 by -0.04 day per spring, significant at the 95% confidence level. Therefore, changes in total frequency of typical circulation patterns has the ability to explain the decreasing long-term trend in DSF over the TD in 1958–2007, which provided a reliable way to project future dust storm over the TD in the warming scenarios.

Then we evaluated the performance of the CMIP6 models in reproducing the long-term changes in the total frequency of typical circulation patterns during 1958–2007. Figure 3(a) shows the distribution of frequency of typical circulation pattern derived from the JRA-55 Reanalysis dataset and from the 13 CMIP6 models. The JRA-55 Reanalysis dataset showed that C2 and C4 had the highest frequency by more than 6 days per spring and C3 had the lowest frequency by less than 1 days per spring. The frequency of typical circulation pattern of C1 was less than 3 days per spring. By comparing the distribution of frequency of typical circulation patterns from the CMIP6 models with the JRA-55 Reanalysis dataset, the MME of CMIP6 models captured the distribution of frequency of typical circulation patterns revealed by the JRA-55 Reanalysis dataset.



By comparing the linear-trend in the total frequency of typical circulation patterns from the CMIP6 models with that from the JRA-55 Reanalysis dataset during 1958–2007, there were seven models showing negative trends in the total frequency of typical circulation patterns (CMCC-CM2-SR5, CMCC-ESM2, CNRM-CM6-1, EC-Earth3-Veg-LR, IPSL-CM6A-LR, NorESM2-MM, and UKESM1-0-LL). The MME of these seven CMIP6 models also showed similar distribution of frequency of typical circulation patterns as well as the JRA-55 Reanalysis dataset (figure S4). The composite of high-pass filtered Z500 of typical circulation patterns from these seven models highly resembled those derived by SOM (figure S5). The MME of the total frequency of typical circulation patterns derived from the seven CMIP6 models presented a decreasing trend by -0.4 day per 10 springs during 1958–2007, significant at the 95% confidence level (figure 3(c)). Thus, we will use these seven models to project the changes in the frequency of typical circulation patterns in 2015–2100 under a warming scenario SSP5-85.

3.3. Increasing frequency of typical circulation pattern in the future

Figure 4 shows the MME of frequency of typical circulation patterns in the future derived from seven CMIP6 models. The frequency of C1–C4 in 2016–2100 presents similar distributions as well as that in 1958–2014, i.e., the highest frequency of C2 and C4 followed by C1 and the lowest one of C3. Compared with 1958–2014, the median of frequency of C2 and C4 will increase in 2076–2095. It implies that the frequency of C2 and C4 will increase in the latter half of the 21st century. However, the frequency of C3 will not change in the future compared with 1958–2014.

We then derived the time series of total frequency of typical circulation patterns from 1958–2100. The frequency shows a decreasing trend from 1958 to 2020. Then the frequency will increase from 2020 to 2100 (figure 4(b)). The typical circulation patterns occurred 17.6 days per spring in 1958–2014 and 20.9 days per spring in 2076–2095. The frequency of typical circulation patterns in the latter half of this century implies an increase in dust storms over the TD under an extreme warming scenario, which is caused by the increase in the frequency of C2 and C4.

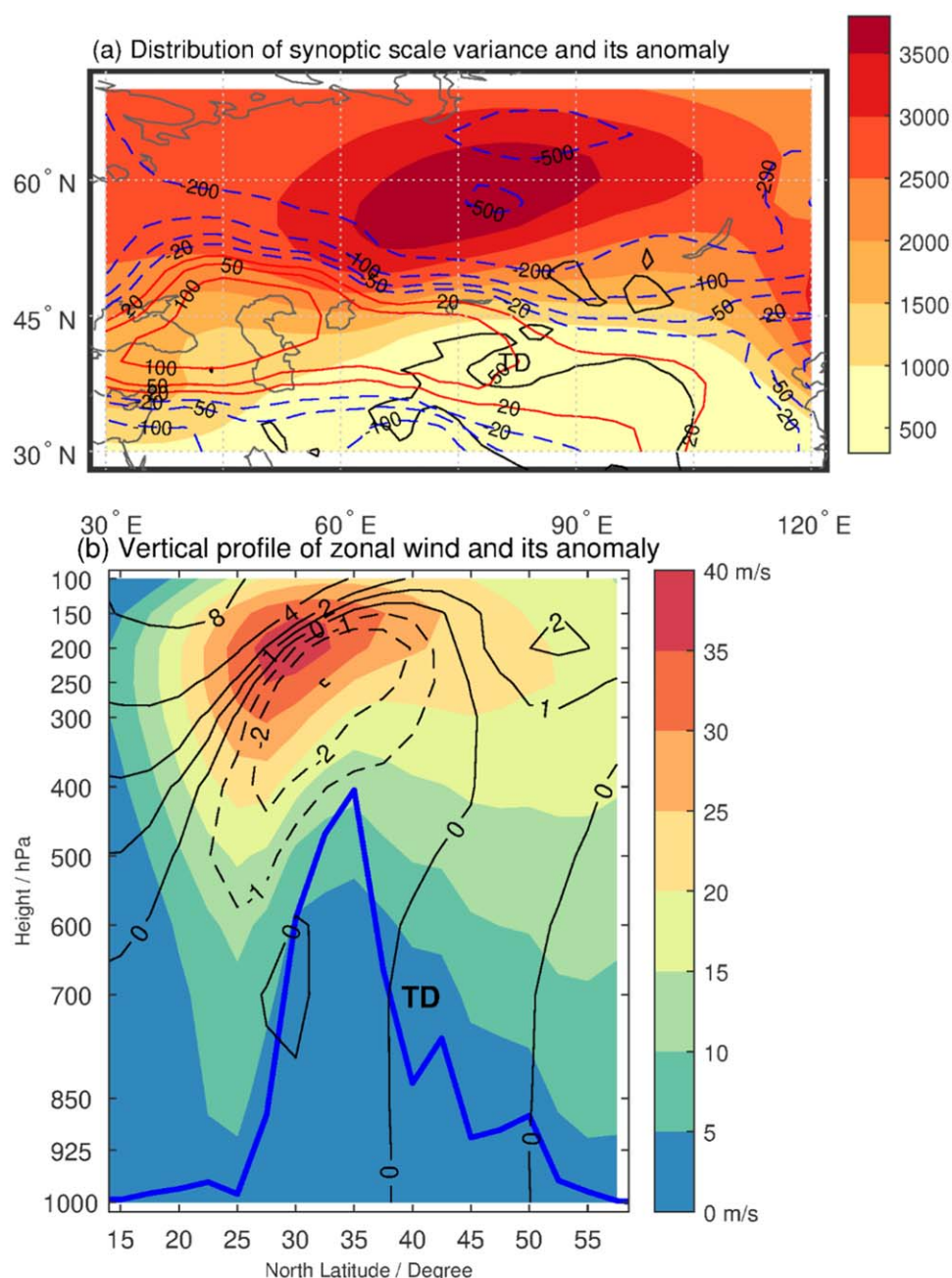


Figure 5. Difference in synoptic-scale disturbance at 500 hPa level (a) and the vertical profile of zonal wind (b) between 1958–2014 and 2076–2095 derived from EC-Earth3-Veg-LR and NorESM2-LM model (2076–2095 minus 1958–2014). The vertical profile of zonal wind is horizontally averaged between 75°E–95°E over the Taklimakan Desert (TD). Synoptic-scale disturbance in the middle troposphere reflects synoptic activity that controls dust storms. The synoptic-scale disturbance is measured with a variance of high-pass filtered Z500 less than 10 days periods. Colored shaded area indicates climatological synoptic-scale disturbance (a) and horizontally averaged zonal winds (b) during 1958–2014. The difference is illustrated by contours in (a) and (b) with positive (negative) values shown by solid lines (dashed lines). The unit is m^2 in (a) and m s^{-1} in (b). The heavy blue line in (b) presents the vertical profile of topographical height between 75°E–95°E.

4. Discussions

To explain the increase in the frequency of typical circulation pattern in the future, we examined changes in synoptic-scale disturbance at 500 hPa level. We firstly examined the climatology of synoptic-scale disturbances at 500 hPa level during 1958–2014, which was featured by a horizontal belt of high values in the middle to high latitudes from Europe to East Asia and low values in the low latitudes from Middle Asia to the Tibetan Plateau (only two models used for simplicity, EC-Earth3-Veg-LR and NorESM2-LM). Figure 5(a) shows the difference in synoptic-scale disturbances between 1958–2014 and 2076–2095 (the latter minus the former). As to compare with 1958–2014, there is an increase in the synoptic-scale disturbances over the middle Asia and a decrease in the synoptic-scale disturbances in the middle to high latitudes. The decreased synoptic-scale disturbances in the

middle to high latitudes may result in decreased synoptic activities from high latitudes to northern China and hence decreased dust storms in the TD. However, the increased synoptic-scale disturbances over the Middle Asia was consistent to the increase in the frequency of C2 in 2076–2095, which may increase the possibility of synoptic activities in the Middle Asia and hence increase dust storms in the TD.

Mid-latitude synoptic activity such as extratropical cyclones or perturbations is related to variations in upper-tropospheric jets (Christenson *et al* 2017). To explain the increased synoptic-scale disturbances at 500 hPa level over the Middle Asia and the TD, we examined a vertical profile of horizontally averaged differences in zonal winds over the TD (75°E–95°E) between 1958–2014 and 2076–2095 (the latter minus the former, figure 5(b)). The results confirmed a significantly southern displacement of subtropical westerly jet stream in the high troposphere to the south of the Tibetan Plateau in 2076–2095 as to compare with 1958–2014, which may be related to the southern displacement of high synoptic-scale disturbances and hence the increase in the synoptic-scale disturbances in the middle troposphere over the TD.

5. Conclusions

Synoptic-scale circulation in the middle troposphere plays an important role in generating dust storms over the TD, northwest China, by inducing strong winds into the Tarim Basin. Four typical circulation patterns in association with dust storms over the TD in spring, called C1 to C4, were identified by using self-organizing maps (SOMs) method. C2, C3, and C4 showed a trough to the northwest of the TD, to the north of the TD, and to the northeast of the TD, respectively. C1 was featured by a ridge to the northeast of the Altai Mountains and a trough to the east of the Ural Mountains. Since the blocking effect of the Altai Mountains, surface winds before the trough in the C1–C3 and those after the trough in the C4 moved into the corridor between the Altai Mountain and the Tianshan Mountain and then turned eastward into the TD due to the blocking effect of the Tibetan Plateau. C1, C2, and C4 were more responsible for DSF over the TD with more frequent occurrence of typical circulation pattern associated with them.

The MME of total frequency of typical circulation patterns derived from seven CMIP6 models showed a decreasing trend in 1958–2007, as shown in the observations. Compared with historical period (1958–2014), there will be an increase in the total frequency of circulation pattern in the latter half of the 21st century under the SSP5–8.5 warming scenario, mainly caused by the increase in the frequency of C2 and C4. The increase in the total frequency of typical circulation patterns in the future implies an increase in dust storms over the TD in the future under the SSP5–85 scenario. The increases in the frequency of typical circulation patterns may be related to an increase in synoptic-scale disturbances over the Middle Asia in the future, caused by a southern displacement of subtropical westerly jet stream in the future compared to historical periods.

Acknowledgments

We thank Dr Ming Bao (School of Atmospheric Sciences, Nanjing University, China) for providing codes for SOM analysis. The authors thank to two anonymous reviewers and editors for their insightful comments. This study was supported by the China's Second Tibetan Plateau Scientific Expedition and Research (2019QZKK0906), the National Key Research and Development Program (2020YFA0608201), and Project PE21030 of the Korea Polar Research Institute. Zhang was supported by the West Light Foundation of the Chinese Academy of Sciences (no.2020-XBQNXZ-015). Mao was supported by the NSFC (41730639, 41571039).

Data availability statement

The data that support the findings of this study are available upon reasonable request from the authors.

ORCID iDs

Rui Mao  <https://orcid.org/0000-0003-1310-0839>

Seong-Joong Kim  <https://orcid.org/0000-0002-6232-8082>

References

Aoki I, Kurosaki Y, Osada R, Sato T and Kimura F 2005 Dust storms generated by mesoscale cold fronts in the Tarim Basin, Northwest China *Geophys. Res. Lett.* **32** L06807

- Bao M and Wallace J M 2015 Cluster analysis of northern hemisphere wintertime 500-hPa flow regimes during 1920–2014 *J. Atmos. Sci.* **72** 3597–608
- Chen S, Huang J, Zhao C, Qian Y, Ruby Leung L and Yang B 2013 Modeling the transport and radiative forcing of Taklimakan dust over the Tibetan plateau: a case study in the summer of 2006 *J. Geophys. Res.* **118** 797–812
- Christenson C E, Martin J E and Handlos Z J 2017 A synoptic climatology of Northern Hemisphere, cold season polar and subtropical jet superposition events *J. Climate* **30** 7231–46
- Gong D Y, Mao R and Fan Y D 2006 East Asian dust storm and weather disturbance: Possible links to the Arctic Oscillation *Int. J. Climatol.* **26** 1379–96
- Han Y, Fang X, Zhao T, Bai H, Kang S and Song L 2009 Suppression of precipitation by dust particles originated in the Tibetan Plateau *Atmos. Environ.* **43** 568–74
- Huang J, Minnis P, Yi Y, Tang Q, Wang X, Hu Y, Liu Z, Ayers K, Trepte C and Winker D 2007 Summer dust aerosols detected from CALIPSO over the Tibetan Plateau *Geophys. Res. Lett.* **34** L18805
- Harada Y, Kamahori H, Kobayashi C, Endo H, Kobayashi S, Ota Y, Onoda H, Onogi K, Miyaoka K and Takahashi K 2016 The JRA-55 Reanalysis: Representation of atmospheric circulation and climate variability *J. Meteor. Soc. Japan* **94** 269–302
- Kobayashi S *et al* 2015 The JRA-55 Reanalysis: General Specifications and Basic Characteristics *Journal of the Meteorological Society of Japan. Ser. II* **93** 5–48
- Jiang Y, Zhang Q-F, Zhao X-N, Wang L and Xiang Z 2018 A geogrid-based framework of agricultural zoning for planning and management of water & land resources: a case study of northwest arid region of China *Ecol. Indic.* **89** 874–79
- Kim T-H, Boo K-O, Lee J and Cho C 2014 Analysis of the future emission changes in mineral dust aerosol in CMIP5 related to bare soil and soil moisture conditions *J. Climate Res.* **9** 33–51
- Lee S and Feldstein S B 2013 Detecting ozone- and greenhouse gas-driven wind trends with observational data *Science* **339** 563–67
- Mao R, Gong D, Bao J and Fan Y 2011a Possible influence of Arctic Oscillation on dust storm frequency in North China *J. Geographical Sci.* **21** 207–18
- Mao R, Ho C-H, Shao Y, Gong D-Y and Kim J 2011b Influence of Arctic Oscillation on dust activity over northeast Asia *Atmos. Environ.* **45** 326–37
- O'Neill B C *et al* 2016 The scenario model intercomparison project (ScenarioMIP) for CMIP6 *Geosci. Model Dev.* **9** 3461–82
- Pu B and Ginoux P 2018 How reliable are CMIP5 models in simulating dust optical depth *Atmos. Chem. Phys.* **18** 12491–510
- Sun J M, Zhang M Y and Liu T S 2001 Spatial and temporal characteristics of dust storms in China and its surrounding regions, 1960–1999: Relations to source area and climate *J. Geophys. Res.* **106** 10,325–33
- Tsunematsu N, Kuze H, Sato T, Hayasaki M, Cui F and Kondoh A 2011 Potential impact of spatial patterns of future atmospheric warming on Asian dust emission *Atmos. Environ.* **45** 6682–95
- Uno I, Eguchi K, Yumimoto K, Takemur T, Shimizu A, Uematsu M, Liu Z, Wang Z, Hara Y and Sugimoto N 2009 Asian dust transported one full circuit around the globe *Nature Geosci.* **2** 557–60
- Wang N and Yin J 2019 Self-organizing map network-based precipitation regionalization for the Tibetan Plateau and regional precipitation variability *Theor. Appl. Climatol.* **135** 29–44
- Zhang X Y, Gong S L, Zhao T L, Arimoto R, Wang Y Q and Zhou Z J 2003 Sources of Asian dust and role of climate change versus desertification in Asian dust emission *Geophys. Res. Lett.* **30** 2272
- Zhao Y, Huang A, Zhu X, Zhou Y and Huang Y 2013 The impact of the winter North Atlantic Oscillation on the frequency of spring dust storms over Tarim Basin in northwest China in the past half-century *Environ. Res. Lett.* **8** 024026
- Zhou Z J and Zhang G C 2003 Typical severe dust storms in northern China during 1954–2002 *Chinese Sci. Bull.* **48** 2366–70
- Zong Q, Mao R, Gong D-Y, Wu C, Pu B, Feng X and Sun Y 2021 Changes in dust activity in spring over East Asia under a Global Warming Scenario *Asia-Pacific J. Atmos. Sci.* **57** 839–50